

# The Slot-Coupled Hemispherical Dielectric Resonator Antenna With a Parasitic Patch: Applications to the Circularly Polarized Antenna and Wide-Band Antenna

Kwok Wa Leung, *Senior Member, IEEE*, and Hoi Kuen Ng

**Abstract**—The aperture-coupled hemispherical dielectric resonator antenna (DRA) with a parasitic patch is studied rigorously. Using the Green's function approach, integral equations for the unknown patch and slot currents are formulated and solved using the method of moments. The theory is utilized to design a circularly polarized (CP) DRA and a wide-band linearly polarized (LP) DRA. In the former, the CP frequency and axial ratio (AR) can easily be controlled by the patch location and patch size, respectively, with the impedance matched by varying the slot length and microstrip stub length. It is important that the AR will not be affected when the input impedance is tuned, and the CP design is therefore greatly facilitated. For the wide-band LP antenna, a maximum bandwidth of 22% can be obtained, which is much wider than the previous bandwidth of 7.5% with no parasitic patches. Finally, the frequency-tuning characteristics of the proposed antenna are discussed. Since the parasitic patch can be applied to any DRAs, the method will find applications in practical DRA designs.

**Index Terms**—Author, please supply your own keywords or send a blank e-mail to keywords@ieee.org to receive a list of suggested keywords.

## I. INTRODUCTION

FOR many years, significant research effort has been devoted to the study of the circularly polarized (CP) antenna. This is because, when compared with the linearly polarized (LP) system, the CP system allows a more flexible orientation between the transmitting and receiving antennas. In addition, CP fields are less sensitive to the propagation effect than LP fields. As a result, the CP system is widely used in satellite communications. In the last decade, excitation of CP fields has been a popular topic in the research of dielectric resonator antennas (DRAs) [1]–[6]. A simple and straightforward CP DRA design is to use a quadrature feed [1]–[3], but this substantially increases the size and complexity of the feed network. Petosa *et al.* [4] shifted the complexity from the feed network to the DRA, but the special-shaped DRA may not be available in the commercial market. To avoid these problems, a parasitic patch has recently been used to obtain the conformal-strip fed CP DRA

[5], [6]. The use of a parasitic patch on the DRA was first considered by Li *et al.* [7] and later by Chen *et al.* [8]. In their work, the parasitic patch was placed on top of a DRA, its purpose being mainly to tune the operating frequency instead of exciting CP fields. Lately, the use of a parasitic patch for the excitation of CP fields has been extended to aperture-coupled sources [9]–[11]. In this paper, we will rigorously study the aperture-coupled DRA with a parasitic patch. It is found that the new configuration is superior to the previous CP DRAs [5], [6] in that a good match can easily be obtained at the CP operating point, which is very important for practical applications. By varying the parameters of the configuration, the CP operating point can be tuned to a certain extent, which is a great advantage over previous aperture-coupled CP DRAs [12]–[15]. In this paper, we will explain the principle behind the CP operation. The effects of the patch and slot parameters on the CP characteristics are examined. Measurements were carried out to verify the theory, and reasonable agreement between theory and experiment is obtained.

Depending on the patch location, the configuration can also be used as a linearly polarized (LP) wide-band antenna. The research of the wide-band DRA was first done in 1989 by Kishk *et al.* [16], who stacked two different DRAs on top of one another to obtain a dual-resonance operation. Since then other wide-band DRAs using stacking methods have been reported [17]–[19]. Alternatively, Simon and Lee [20] and Z. Fan *et al.* [21] placed two parasitic DR elements beside the DRA to increase the impedance bandwidth. All these wide-band configurations, however, require extra DR elements. Some methods that need only a single DRA were reported. For example, an airgap [22] or a conductor [23] can be introduced inside a DRA to widen the impedance bandwidth. Alternatively, a dielectric coating [24], [25] can be put outside the DRA to obtain a wide-band antenna. Lately, Kishk *et al.* achieved a wide impedance bandwidth by using a conical DRA [26]. The above methods have a drawback that the special DRAs are not readily available in the commercial market. Recently, a parasitic patch has been employed to increase the impedance bandwidth, with the DRA fed by a probe or a conformal strip [6], [27]. This new approach is more convenient than the previous ones because it merely requires a simple DRA. In this paper, the LP wide-band characteristics of the proposed configuration are also investigated theoretically and experimentally. It is found that the bandwidth of

Manuscript received July 7, 2003; revised July 11, 2004. The work was supported by a grant from the Research Grant Council of the Hong Kong Special Administrative Region, China under Project CityU 1178/01E.

The authors are with the Wireless Communications Research Centre and Department of Electronic Engineering, City University of Hong Kong, Kowloon, Hong Kong (e-mail: eekleung@cityu.edu.hk).

Digital Object Identifier 10.1109/TAP.2005.846731

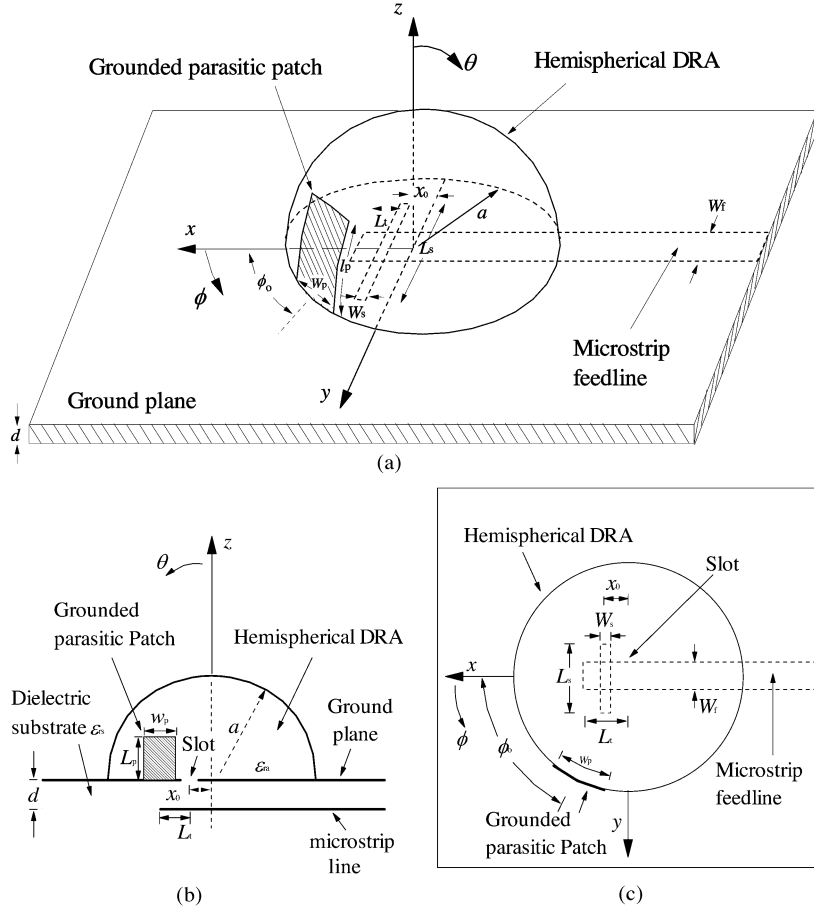


Fig. 1. Configuration of the aperture-coupled hemispherical DRA with a parasitic patch. (a) Perspective view. (b) Side view. (c) Top view.

the DRA can be more than 22%, which is about 3 times of that without the parasitic patch [11]. The effects of the patch and slot parameters on the wide-band characteristics are studied. Again, measurements were done to verify the theory, with good results. It should be mentioned that the parasitic patch, like [7], [8], can also be used as frequency-tuning element. Although in this case the bandwidth is reduced to about 13%, it is still about twice the bandwidth without the parasitic patch. The frequency-tuning capability will be addressed in this paper as well.

In this paper, the Green's function approach is used to formulate the problem, and the unknown patch and slot currents are solved using the method of moments (MoM). The problem can be divided into two parts, namely the DRA part above the ground plane and the microstrip feedline part below the ground plane, as was done previously in [11]. In the DRA part, the mode-matching method is used to obtain exact DRA Green's functions, whereas the spectral-domain analysis will be used for the feedline part.

## II. FORMULATION

The configuration of the DRA is shown in Fig. 1, where the slot of length  $L_s$  and width  $W_s$  couples the energy from the microstrip line to the hemispherical DRA of radius  $a$  and dielectric constant  $\epsilon_{ra}$ . In general, the slot has offset  $x_0$  from the  $y$ -axis. The slot offset  $y_0$  from the  $x$  axis is not included in this work, as it was previously found [11] that its effect is not as significant as

for  $x_0$ . The parasitic patch of length  $l_p$  and width  $W_p$  is located at angular displacement  $\phi_0$  from the  $x$ -axis. The grounded dielectric slab has dielectric constant  $\epsilon_{rs}$  and height  $d$ , on which a microstrip feedline of width  $W_f$  and stub length  $L_t$  is fabricated. In the following formulation, the fields are assumed to vary harmonically as  $e^{j\omega t}$ , and  $\vec{r}$  and  $\vec{r}'$  refer to the field and source coordinates, respectively. Let  $M_y$  be the equivalent magnetic current in the slot, and  $J_\theta$ ,  $J_\phi$  be the electric current components of the parasitic patch. To begin with, we enforce the boundary condition that the electric field components  $E_\theta$ ,  $E_\phi$  should vanish on the parasitic patch. Mathematically, we have

$$E_{J_\theta}^{\theta,\phi} + E_{J_\phi}^{\theta,\phi} = -E_{M_y}^{\theta,\phi} \quad (1)$$

where the superscripts and subscripts describe the field components and the current sources that produce the field components, respectively. Using the MoM, the magnetic and electric currents are expanded as follows:

$$M_y(x, y) = \sum_{n=1}^{N_1} V_n f_n(x, y) \quad (2)$$

$$J_{\theta,\phi}(\theta) = \sum_{p=1}^{N_{2,3}} I_{\theta,\phi p} g_{\theta,\phi p}(\theta) \quad (3)$$

where the basis function  $f_n(x, y)$  was defined in [11] and  $g_{\theta p}(\theta)$ ,  $g_{\phi p}(\theta)$  are piecewise sinusoidal (PWS) basis functions.

Applying the Galerkin's procedure, the following matrix equation is obtained:

$$\begin{bmatrix} [Z_{\theta\theta}]_{N_2 \times N_2} & [Z_{\theta\phi}]_{N_2 \times N_3} \\ [Z_{\phi\theta}]_{N_3 \times N_2} & [Z_{\phi\phi}]_{N_3 \times N_3} \end{bmatrix} \begin{bmatrix} [I_{\theta p}]_{N_2 \times 1} \\ [I_{\phi q}]_{N_3 \times 1} \end{bmatrix} = \begin{bmatrix} [A_{\theta}]_{N_2 \times 1} \\ [A_{\phi}]_{N_3 \times 1} \end{bmatrix} [V_n] \quad (4)$$

where, for  $\alpha, \beta = \theta$  or  $\phi$

$$Z_{\alpha\beta} = \frac{-1}{\Gamma_\alpha \Gamma_\beta} \iint_{S_p} \iint_{S_p} g_{\alpha p}(\alpha) G_{J_\beta}^{E_\alpha} g_{\beta q}(\beta') dS' dS \quad (5)$$

and

$$A_\alpha = \frac{1}{\Gamma_\alpha} \iint_{S=S_p} \iint_{S'=S_o} g_{\alpha p}(\alpha) G_{M_y}^{E_\alpha} f_n(x', y') dS' dS \quad (6)$$

in which  $\Gamma_\theta = W_p$  and  $\Gamma_\phi = L_p$ , and  $G_{J_\alpha}^{E_\beta}$  ( $\alpha, \beta = \theta$  or  $\phi$ ) and  $G_{M_y}^{E_\beta}$  are the Green's functions of  $E_\beta$  due to point currents of  $J_\alpha$  and  $M_y$ , respectively. Since the current vectors  $[I_{\theta p}]$ ,  $[I_{\phi q}]$  (or  $[I_{\phi p}]$  since  $p, q$  are indexes only) are uncoupled in (4), each of them can be expressed in terms of  $[V_n]$  as follows:

$$[I_{\alpha p}] = [\Omega_\alpha][V_n], \quad \alpha = \theta, \phi \quad (7)$$

where

$$\Omega_\theta = \left[ [I] - [Z_{\phi\phi}]^{-1} [Z_{\theta\phi}] [Z_{\phi\phi}]^{-1} [Z_{\phi\theta}] \right]^{-1} \cdot \left[ [Z_{\theta\theta}]^{-1} [\Psi_\theta] - [Z_{\theta\theta}]^{-1} [Z_{\theta\phi}] [Z_{\phi\phi}]^{-1} [A_\phi] \right] \quad (8)$$

$$\Omega_\phi = \left[ [I] - [Z_{\theta\theta}]^{-1} [Z_{\phi\theta}] [Z_{\theta\theta}]^{-1} [Z_{\phi\phi}] \right]^{-1} \cdot \left[ [Z_{\phi\phi}]^{-1} [\Psi_\phi] - [Z_{\phi\phi}]^{-1} [Z_{\phi\theta}] [Z_{\theta\theta}]^{-1} [A_\theta] \right]. \quad (9)$$

In (8), (9), the matrix elements  $Z_{\alpha\beta}$  are equal to  $Z_{\alpha\beta}^{BB'}$  given in [5], which can efficiently be evaluated using recurrence formulas, and  $[I]$  is the identity matrix.

From (7), we have two sets of equations for three sets of unknowns, namely  $[I_{\theta p}]$ ,  $[I_{\phi p}]$ , and  $[V_n]$ . The third set of equation comes from matching the boundary condition that the magnetic field  $H_y$  is continuous across the slot, and the equation is given below

$$\left\{ [Y_{mn}^a - Y_{mn}^s] + \frac{1}{2} [\Delta v_m] [\Delta v_n]^t \right\} [V_n] + [B_\theta] [I_{\theta p}] + [B_\phi] [I_{\phi p}] = [\Delta v_m] \quad (10)$$

where, for  $\alpha = \theta$  or  $\phi$

$$B_\alpha = \frac{1}{\Gamma_\alpha} \iint_{S=S_o} \iint_{S'=S_p} f_m(x, y) G_{J_\alpha}^{H_y} g_{\alpha p}(\alpha') dS' dS \quad (11)$$

and  $Y_{mn}^a$ ,  $Y_{mn}^s$ , and  $\Delta v_m$  are the DRA admittance with no parasitic patches, the substrate admittance, and the discontinuity voltage of the slot, respectively. Finally, insertion of (7) into (10) gives the coefficient matrix  $[V_n]$  of the magnetic current as follows:

$$[V_n] = \left\{ [Y_{mn}^b - Y_{mn}^s] + \frac{1}{2} [\Delta v_m] [\Delta v_n]^t \right\}^{-1} [\Delta v_m] \quad (12)$$

where

$$[Y_{mn}^b] = [Y_{mn}^a] + [B_\theta][\Omega_\theta] + [B_\phi][\Omega_\phi]. \quad (13)$$

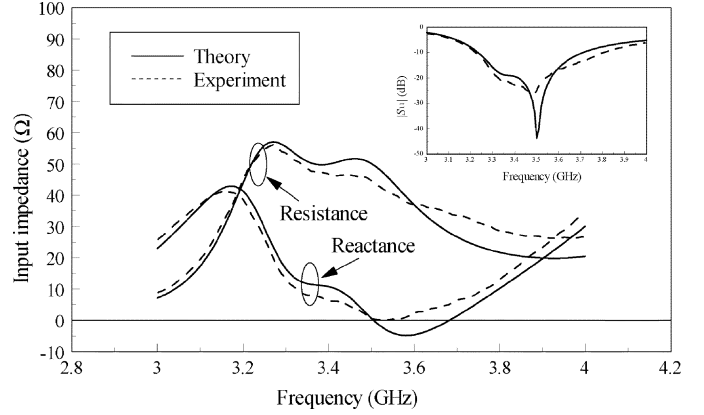


Fig. 2. Measured and calculated input impedances as a function of frequency:  $a = 12.5$  mm,  $\epsilon_{ra} = 9.5$ ,  $L_s = 13.2$  mm,  $W_s = 1$  mm,  $x_0 = 0$  mm,  $l_p = 7.62$  mm,  $W_p = 2.1$  mm,  $\phi_0 = 55^\circ$ ,  $L_t = 11.4$  mm,  $W_f = 4.7$  mm,  $\epsilon_{rs} = 2.33$ ,  $d = 1.57$  mm,  $N_1 = N_2 = 5$ ,  $N_3 = 3$ . The inset shows the corresponding measured and calculated  $|S_{11}|$ .

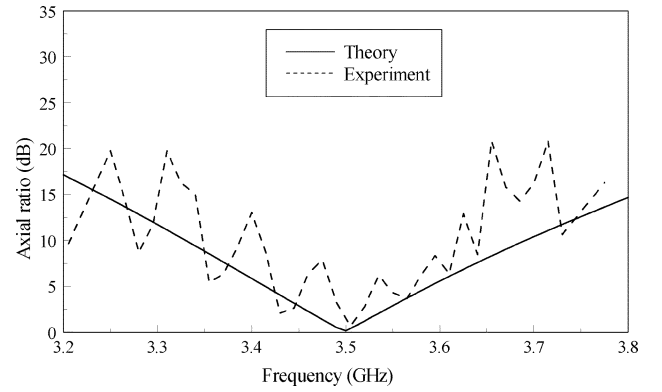


Fig. 3. Measured and calculated axial ratios as a function of frequency. The parameters are the same as in Fig. 2.

It should be noted that the result (12) has exactly the same form as the previous one [11]. When the parasitic patch is vanishingly small, we have  $[I_{\theta p}] = [I_{\phi p}] = [0]$ , leading to  $[\Omega_\theta] = [\Omega_\phi] = [0]$  from (7). In this case  $[Y_{mn}^b] = [Y_{mn}^a]$  and (12) is reduced to the previous result [11], which is to be expected. After  $[V_n]$  is found, the input impedance and radiation fields can be calculated easily.

### III. CP OPERATION MODE

The CP operation mode of the configuration is discussed first. For simplicity, the slot is placed centrally ( $x_0 = 0$ ) throughout this part. The parasitic patch generates two orthogonal field components. One of the field components is combined with the slot field. When the patch has a proper patch size and location, the remaining field component and the combined field can be of the same magnitude but of  $90^\circ$  phase difference, thus generating CP fields.

The effect of patch length  $l_p$  on the axial ratio (AR) was studied. Three different sets of slot length  $L_s$  and stub length  $L_t$  that give a good impedance match at 3.5 GHz were used. It was observed that the three sets of results were completely overlapped, showing that the AR is not affected by  $L_s$  and  $L_t$ . This is very important, since it suggests that after the AR is designed, we can tune the impedance by varying  $L_s$  and  $L_t$  without affecting the AR. The result greatly facilitates the CP antenna de-

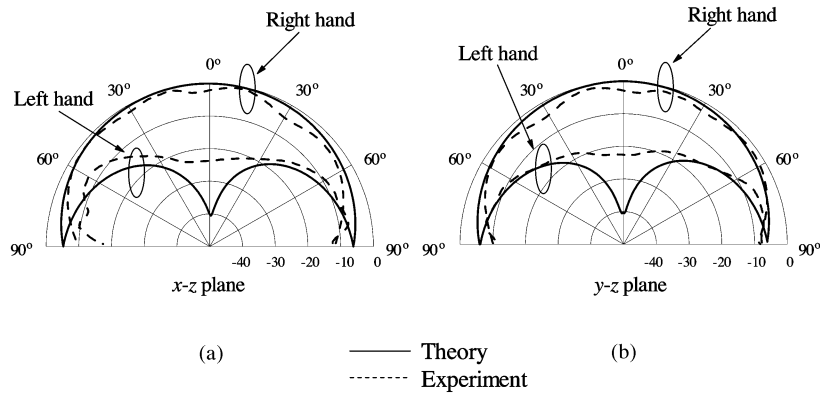


Fig. 4. Measured and calculated radiation patterns of the CP DRA at 3.50 GHz. The parameters are the same as in Fig. 2. (a)  $xz$ -plane. (b)  $yz$ -plane.

sign. It was found that  $l_p$  strongly affects the level of the AR. The corresponding minimum-AR frequency point,  $f_{\min}$ , was also studied, which decreases with increasing  $l_p$ . It should be pointed out that the minimum AR point is different from the optimum AR point where  $AR < 0.1$  dB. It is interesting that the latter only depends on the patch location  $\phi_0$ , which will be discussed later in more detail.

Fig. 2 displays the measured and calculated input impedances of the DRA, with reasonable agreement between theory and experiment. In the measurement, a rectangular parasitic patch of  $l_p = 7.62$  mm,  $W_p = 2.1$  mm was cut from a conducting adhesive tape. The parasitic patch was stuck on the DRA surface directly. An HP8510C network analyzer was used to measure the antenna, with the reference plane set at the center of the coupling slot. A relatively large discrepancy is found at relatively high frequencies. Apart from experimental tolerances, an error was introduced by the fact that the theory assumes a varying patch width along the meridian plane but a constant patch width was used in the measurement. This error should be more significant around the patch resonance. The inset shows the corresponding measured and calculated return losses. Both of them are maximum at  $f = 3.50$  GHz, which is around the DR  $TE_{111}$ -mode resonance. The measured and calculated impedance bandwidths ( $|S_{11}| < -10$  dB) are 16 and 14%, respectively, which are much wider than 7.5% for the DRA without the parasitic patch [11].

Fig. 3 shows the measured and calculated AR's of the DRA. Again, reasonable agreement between theory and experiment is obtained. The ripple of the measured result is primarily caused by the finite ground plane. From the figure, the calculated 3-dB AR bandwidth is given by 3.4%, which is higher than 2.4% for the previous conformal-strip fed version [5]. It is important to note that the optimum AR is found at  $f = 3.50$  GHz, which is also the optimum return loss of the antenna. This is a very desirable result for practical CP designs.

The measured and calculated radiation fields at  $f = 3.50$  GHz are plotted in Fig. 4, where the calculation agrees reasonably with the measurement. With reference to the figure, a typical broadside  $TE_{111}$ -mode pattern is observed. The DRA is a right-hand CP (RHCP) antenna, and that a left-hand CP (LHCP) antenna should be obtained if the parasitic patch

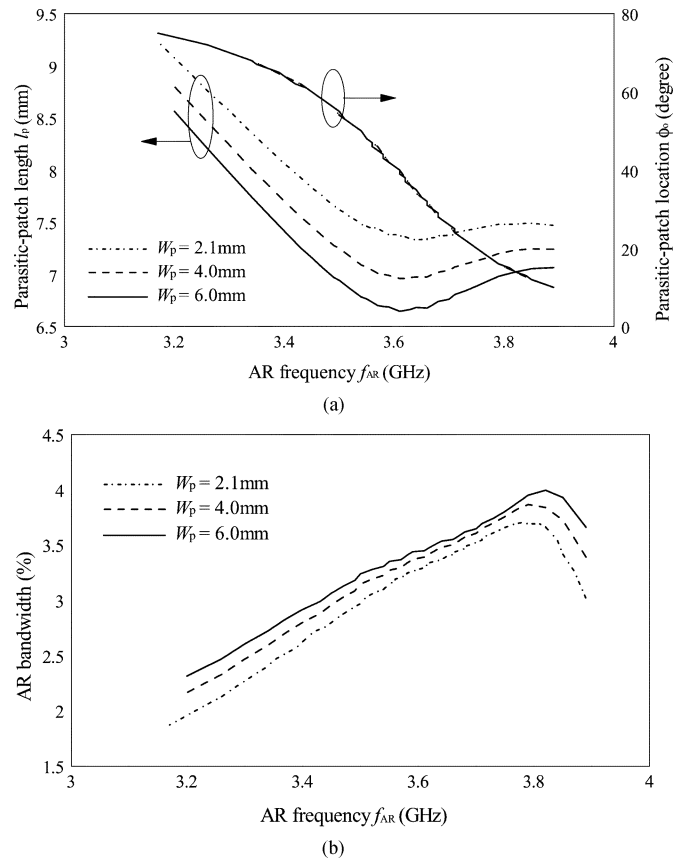


Fig. 5. Patch length  $l_p$ , patch location  $\phi_0$  and AR bandwidth as a function of AR frequency for  $W_p = 2.1, 4.0$  and  $6.0$  mm. Other parameters are the same as in Fig. 2. (a) Patch length  $l_p$  and location  $\phi_0$ . (b) Axial ratio bandwidth.

is placed at  $305^\circ$ . As can be observed from the figure, the calculated difference between the RHCP and LHCP fields in the broadside direction ( $\theta = 0^\circ$ ) is about 40 dB, which is very sufficient for many applications. The measured result, however, has a smaller difference of about 20 dB due to experimental tolerances. Since the patch location ( $\phi_0 = 55^\circ$ ) is close to the diagonal plane ( $\phi_0 = 45^\circ$ ), the  $xz$  and  $yz$  plane results are very similar to each other for both the RHCP and LHCP fields. The field patterns for  $\phi_0 = 75^\circ$  were plotted, and it was found that the  $xz$  and  $yz$  plane results are significantly different from each other, which is to be expected.

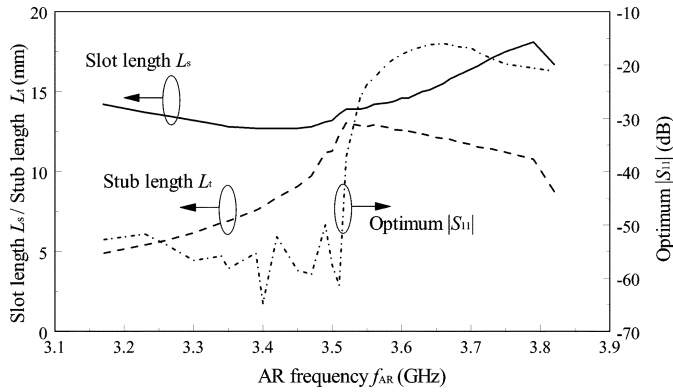


Fig. 6. Slot length  $L_s$  and microstrip stub length  $L_t$  with optimum return loss as a function of AR frequency. The patch length is extracted from Fig. 5(a) with  $W_p = 2.1$  mm. Other parameters are the same as in Fig. 2.

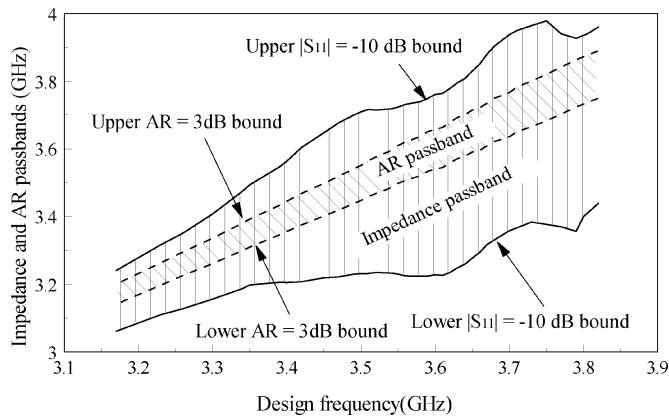


Fig. 7. Impedance and AR passbands as a function of design frequency of the CP DRA. The patch length  $l_p$  is extracted from Fig. 5(a) with  $W_p = 2.1$  mm, whereas the slot length  $L_s$  and microstrip stub length  $L_t$  are extracted from Fig. 6. Other parameters are the same as in Fig. 2.

Fig. 5 shows the required  $l_p$  and  $\phi_0$  to obtain the optimum AR as a function of AR design frequency,  $f_{AR}$ , for  $W_p = 2.1, 4.0,$  and  $6.0$  mm. For each curve, the AR is kept below  $0.1$  dB. With reference to the figure, a higher  $l_p$  is needed for a smaller  $W_p$  so that a certain patch area is maintained. It is interesting to note that the patch location  $\phi_0$  is virtually the same for all the different  $W_p$  and, accordingly,  $l_p$ . This is very important, since it implies that the AR frequency is predominantly determined by  $\phi_0$  instead of the patch size. (Of course, the patch size has to be adjusted to give the optimum AR  $< 0.1$  dB. The key point here is that when  $\phi_0$  is fixed, the optimum AR frequency virtually remains unchanged for different combinations of  $l_p$  and  $W_p$ .) Fig. 5(b) shows the 3-dB AR bandwidth as a function of  $f_{AR}$ . For all the  $W_p$ , the AR bandwidth initially increases with  $f_{AR}$  until  $f_{AR} \sim 3.8$  GHz, after which the bandwidth decreases with increasing  $f_{AR}$ . From the figure, it is observed that the wider the  $W_p$  is, the higher the AR bandwidth.

Next, the impedance matching of the CP DRA is discussed. Fig. 6 shows the tuned slot length  $L_s$  and stub length  $L_t$  that give the optimum return loss. For ease of reference, the corresponding minimum  $|S_{11}|$  is also shown in the figure. In generating the curves, the results of Fig. 5 were used to determine  $l_p$  and  $W_p$  for each frequency and, thus, the condition of AR  $<$

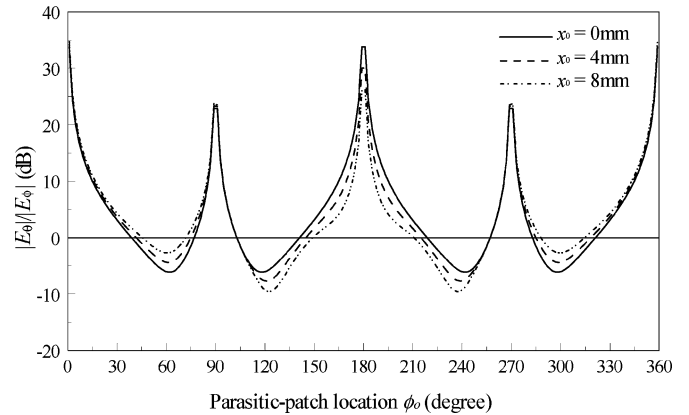


Fig. 8. Crosspolarized field relative to copolarized field as a function of parasitic-patch location for  $x_0 = 0, 4.0$  and  $8.0$  mm in the broadside direction ( $\theta = 0^\circ$ ):  $a = 12.5$  mm,  $\epsilon_{ra} = 9.5$ ,  $L_s = 13$  mm,  $W_s = 1$  mm,  $l_p = 12.0$  mm,  $W_p = 4.0$  mm,  $\phi_0 = 0^\circ$ ,  $L_t = 9.0$  mm,  $W_f = 4.7$  mm,  $\epsilon_{rs} = 2.33$ ,  $d = 1.57$  mm,  $N_1 = N_2 = 5$ ,  $N_3 = 3$ .

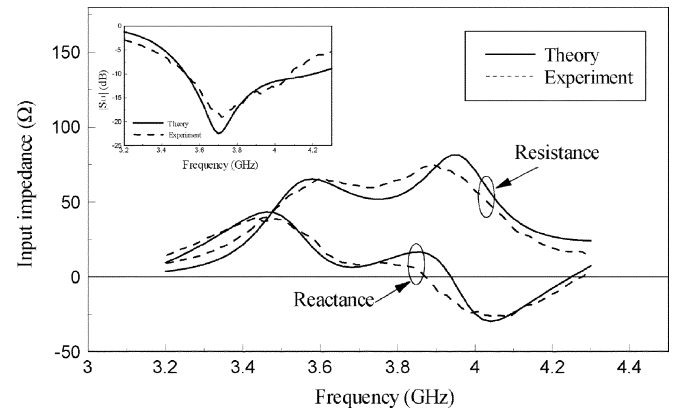


Fig. 9. Measured and calculated input impedances as a function of frequency with  $x_0 = 0$  mm. Other parameters are the same as in Fig. 8. The inset shows the corresponding measured and calculated  $|S_{11}|$ .

$0.1$  dB is ensured. It can be observed that the optimum return loss is higher than  $50$  dB for the frequency range  $3.16 < f_{AR} < 3.51$  GHz, but the optimum return loss is reduced significantly when  $f_{AR} > 3.51$  GHz. Nevertheless, the optimum return loss for  $f_{AR} > 3.51$  GHz is still higher than  $16$  dB, which is acceptable for practical applications. The procedure to achieve an impedance match is very simple. First, adjust the slot length  $L_s$  so that the input resistance is equal to the system impedance ( $50\text{-}\Omega$  in this paper) at the desired frequency, then tune the stub length  $L_t$  to cancel out the reactance. It should be reminded that changing  $L_t$  and  $L_t$  does not affect the AR at all, as discussed previously. (Changing the patch size to tune the AR, however, will affect the input impedance as well. Therefore, the AR should be designed first before the impedance is tuned.) This characteristic is very favorable, since we need to take care of only one parameter at one time.

A CP antenna may not be useful if its impedance passband and AR passband do not overlap. The two passbands as a function of design frequency are examined in Fig. 7. With reference to the figure, the AR passband is kept inside the impedance passband across the whole frequency range, showing that the antenna bandwidth is limited by the AR bandwidth.

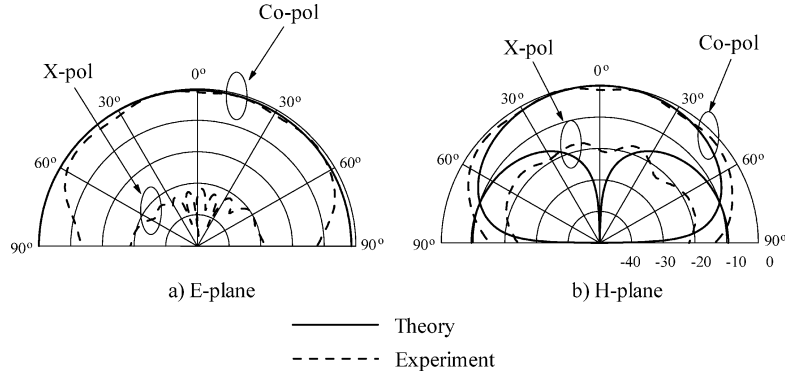


Fig. 10. Measured and calculated radiation patterns of the DRA at 3.70 GHz. Other parameters are the same as in Fig. 8.

#### IV. LP OPERATION MODE

To examine the purity of the LP far fields of the proposed configuration, the far-field ratio of  $E_\theta/E_\phi$  in the  $x$ - $z$  plane (E-plane) is plotted in Fig. 8 for slot offsets  $x_0 = 0, 4,$  and  $8$  mm. At  $\phi_0 = 0^\circ$ , the copolarized field  $E_\theta$  is much stronger than the crosspolarized field  $E_\phi$  due to the symmetry of the patch. Therefore,  $\phi_0 = 0^\circ$  is used throughout this part unless otherwise stated. With reference to the figure,  $\phi_0 = 90^\circ$  also gives a high LP purity. The result is expected, since it was found that the parasitic patch has no effects at this particular location. It can be observed that the  $E_\theta/E_\phi$  ratio is symmetric for  $x_0 = 0$ , and the symmetry is destroyed when  $x_0 \neq 0$ , which is to be expected.

Fig. 9 shows the measured and calculated input impedances for the LP wide-band operation, with  $l_p = 12.0$  mm,  $W_p = 4.0$  mm,  $L_s = 13.0$  mm, and  $W_s = 1.0$  mm. Reasonable agreement between theory and experiment is obtained. Again, as found in the CP case, a relatively large discrepancy is observed at higher frequencies. Two resonant modes are excited, and, thus, the impedance bandwidth is widened. It was found that the first and second resonant modes are the DR resonance and patch resonance, loaded by the slot and DR, respectively. This is different from the CP case in which both the resonant modes are DR modes. The inset shows the measured and calculated  $|S_{11}|$  of the antenna. The measured and calculated frequencies of the minimum  $|S_{11}|$  are 3.71 and 3.70 GHz, respectively, which are very close to the natural frequency of the DR  $TE_{111}$  mode. The measured and calculated bandwidths ( $|S_{11}| < -10$  dB) are 16.2 and 17.5%, respectively. The bandwidths are more than twice the bandwidth without the parasitic patch [11].

The measured and calculated field patterns at  $f = 3.71$  GHz are displayed in Fig. 10, where an expected broadside radiation mode is obtained. With reference to the figure, reasonable agreement between theory and experiment is obtained. It should be mentioned that the calculated crosspolarized field is vanishingly small for the E-plane ( $x$ - $z$  plane) pattern, and that the finite measured result is mainly caused by the finite ground plane diffraction. For the H-plane pattern, the calculated result has a null crosspolarized field in the broadside direction of  $\theta = 0^\circ$ , but, again, a finite measured field is found due to the ground plane diffraction.

Fig. 11 shows the  $|S_{11}|$  as a function of frequency for different  $W_p$ , with  $l_p = 12.0$  mm fixed. It is observed that a wider

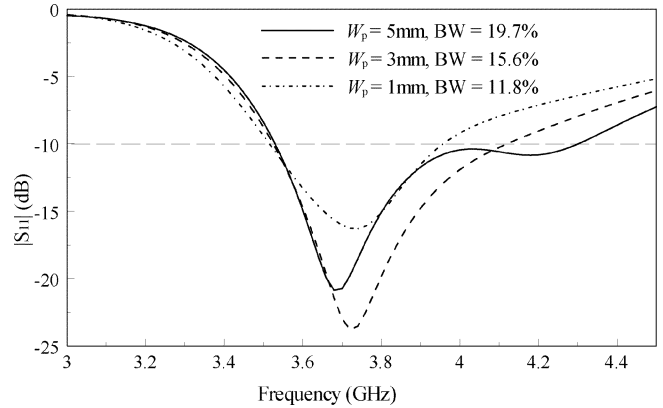


Fig. 11.  $|S_{11}|$  as a function of frequency for  $W_p = 1.0, 3.0,$  and  $5.0$  mm with  $x_0 = 0$  mm. Other parameters are the same as in Fig. 8.

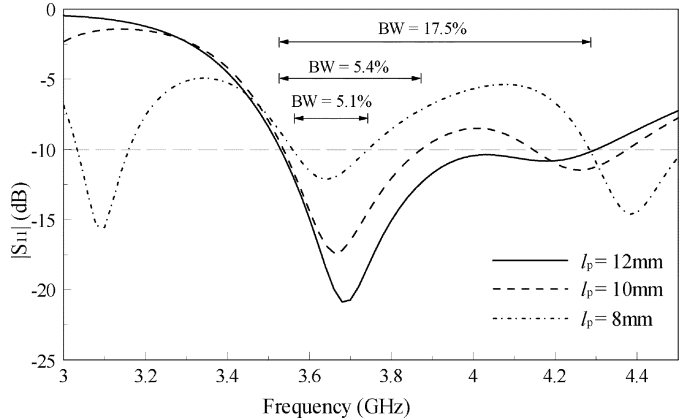


Fig. 12.  $|S_{11}|$  as a function of frequency for  $l_p = 8.0, 10.0$  and  $12.0$  mm with  $x_0 = 0$  mm. Other parameters are the same as in Fig. 8.

$W_p$  gives a wider bandwidth. However, this trend will not continue unlimitedly. This is because, with reference to the curve of  $W_p = 5$  mm, the  $|S_{11}|$  will cross the line of  $|S_{11}| = -10$  dB around  $f \sim 4$  GHz if  $W_p$  is increased further, and, thus, the bandwidth will conversely be reduced.

Fig. 12 shows the  $|S_{11}|$  as a function of frequency for different  $l_p$ , with  $W_p = 5$  mm fixed. The result of  $l_p = 8$  mm is discussed first. Three resonant modes are found. The first ( $\sim 3.10$  GHz), second ( $\sim 3.56$  GHz), and the last ( $\sim 4.3$  GHz) are associated with the patch-loaded DR resonance, slot-loaded DR resonance, and DR-loaded patch resonance, respectively. Since the first and

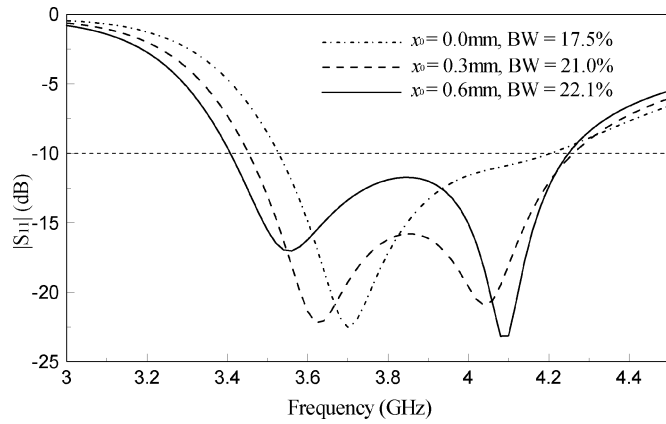


Fig. 13.  $|S_{11}|$  as a function of frequency for  $x_0 = 0.0, 0.3$  and  $0.6$  mm. Other parameters are the same as in Fig. 8.

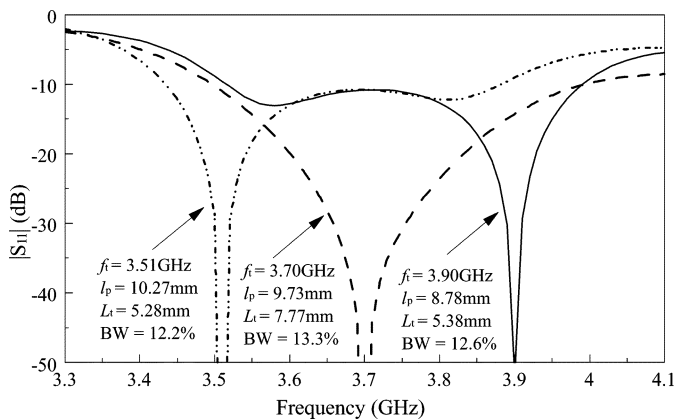
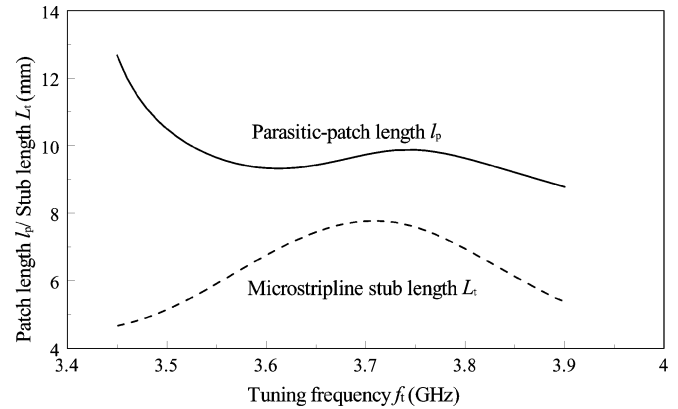


Fig. 14.  $|S_{11}|$  as a function of frequency for the demonstration of frequency tuning. In each case, an excellent impedance match is obtained by choosing a proper  $l_p$  and  $L_t$ . Other parameters are the same in Fig. 8. (i)  $f_t = 3.51$  GHz,  $l_p = 10.27$  mm,  $L_t = 5.28$  mm. (ii)  $f_t = 3.70$  GHz,  $l_p = 9.73$  mm,  $L_t = 7.77$  mm. (iii)  $f_t = 3.90$  GHz,  $l_p = 8.78$  mm,  $L_t = 5.38$  mm.

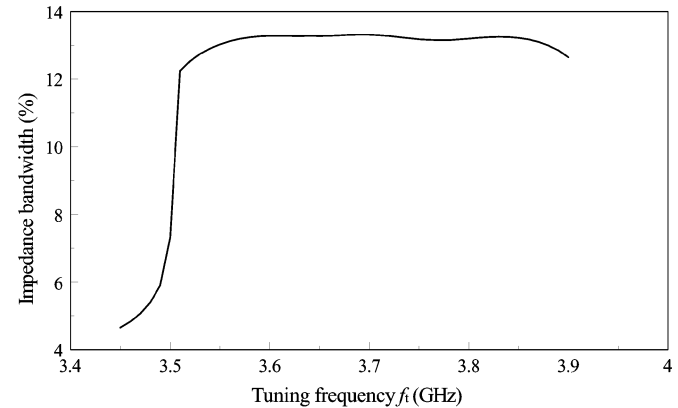
last resonant modes are directly associated with the patch, their resonant frequencies are much more sensitive to  $l_p$  than for the second resonant mode. It is noted that for  $3.5 < f < 4.3$  GHz, quite a large portion of the  $|S_{11}|$  is above the line of  $|S_{11}| = -10$  dB, causing the bandwidth to be relatively narrow. The situation is improved for  $l_p = 10.0$  mm, and that the widest bandwidth is obtained for  $l_p = 12.0$  mm. However, like the result of Fig. 11, the trend will not continue unlimitedly. The reason is that the last resonant mode around 4.3 GHz will move toward the second resonant mode as  $l_p$  increases, which will consequently reduce the impedance bandwidth.

Thus far, the slot has been placed centrally, i.e., offset  $x_0 = 0$ . It is found that with a small offset  $x_0$ , the bandwidth can be increased significantly, as shown in Fig. 13. With reference to the figure, the bandwidth is increased from 17.5% for  $x_0 = 0$  to 21% for  $x_0 = 0.3$  mm. The bandwidth is further increased to 22.1% when  $x_0 = 0.6$  mm. Again, the process cannot be continued unlimitedly, since the  $|S_{11}|$  will cross the line of  $|S_{11}| = -10$  dB around  $f = 3.8$  GHz when  $x_0$  is sufficiently large.

In the previous wide-band results, we have  $|S_{11}| > -25$  dB. The proposed DRA configuration can, of course, give an even better return loss, at the cost of having a reduced bandwidth. We will show some results with excellent impedance



(a)



(b)

Fig. 15. Patch length  $l_p$ , microstrip stub length  $L_t$ , and corresponding impedance bandwidth as a function of tuning frequency with patch width  $W_p = 2.0$  mm. Other parameters are the same as in Fig. 8. (a) Patch length  $l_p$  and microstrip stub length  $L_t$ . (b) Corresponding impedance bandwidth.

matches. Fig. 14 shows three  $|S_{11}|$  curves, each has an excellent impedance match. It is noted that by using different  $l_p$  and  $L_t$ , the frequency of the match point can be tuned. In each case, the bandwidth is about 13%. Although the bandwidth is not as wide as before, it is still about twice the bandwidth of the previous aperture-coupled DRA [11]. The frequency-tuning capability of the configuration is discussed. Fig. 15(a) shows the required  $l_p$  and  $L_t$  as a function of the tuning frequency  $f_t$ , with the corresponding bandwidth given in Fig. 15(b). It is observed that the bandwidth is quite narrow for  $f_t < 3.50$  GHz, but it sharply increases to 12.2% when  $f_t = 3.51$  GHz. After that the bandwidth varies only slightly around 13%.

## V. CONCLUSION

The aperture-coupled hemispherical DRA with a parasitic patch has been studied rigorously, with the DRA excited in its fundamental broadside  $TE_{111}$  mode. The theory has been used to design a CP antenna and a wide-band antenna. In both cases, measurements were carried out to verify the calculations, and reasonable agreement between them has been obtained.

For the CP antenna, it has been found that the design is very easy. First of all, determine from Fig. 5(a) the location of the parasitic patch so that the CP antenna can be operated at the design frequency. Next, use the same figure to determine the patch length  $l_p$  that gives a good AR, with the patch width as

wide as possible to maximize the AR bandwidth. The last step is to match the impedance by choosing the proper  $L_s$  and  $L_t$  from Fig. 6, without the need to worry about the AR that has already been obtained. An axial ratio bandwidth of 3.4% has been found.

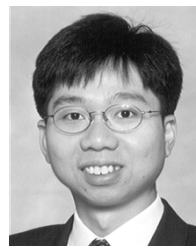
For the wide-band antenna, it has been found that the cross-polarized fields are very weak when the parasitic patch is located at  $\phi_0 = 0$ . When the slot is placed at the center of the DRA, a maximum bandwidth of 19.7% can be obtained, which is 2.6 times of that without the parasitic patch. The bandwidth can further be increased to 22.1% when a small slot offset of  $x_0 = 0.6$  mm is introduced.

The parasitic patch can also be used as a frequency-tuning element. It has been demonstrated that by changing the patch length and microstrip stub length, the operating frequency  $f_0$  can be tuned between 3.45 and 3.90 GHz. The bandwidth is 4.7% at  $f_0 = 3.45$  GHz, and it is about 13% for  $f_0 > 3.51$  GHz.

Finally, it should be reminded that the idea can be applied to other DRAs, and therefore, the results should be very useful to antenna engineers.

#### REFERENCES

- [1] R. K. Mongia, A. Ittipiboon, M. Cuhaci, and D. Roscoe, "Circular polarized dielectric resonator antenna," *Electron. Lett.*, vol. 30, pp. 1361–1362, Aug. 1994.
- [2] G. Drossos, Z. Wu, and L. E. Davis, "Circular polarized cylindrical dielectric resonator antenna," *Electron. Lett.*, vol. 32, pp. 281–283, Feb. 1996.
- [3] K. W. Leung, W. C. Wong, K. M. Luk, and E. K. N. Yung, "Circular-polarized dielectric resonator antenna excited by dual conformal strips," *Electron. Lett.*, vol. 36, no. 6, pp. 484–486, Mar. 2000.
- [4] A. Petosa, A. Ittipiboon, and M. Cuhaci, "Array of circular-polarized cross dielectric resonator antenna," *Electron. Lett.*, vol. 32, pp. 1742–1743, Sep. 1996.
- [5] K. W. Leung and H. K. Ng, "Theory and experiment of circularly polarized dielectric resonator antenna with a parasitic patch," *IEEE Trans. Antennas Propag.*, vol. 51, no. 3, pp. 405–412, Mar. 2003.
- [6] R. T. Long, R. J. Dorris, S. A. Long, M. A. Khayat, and J. T. Williams, "Use of parasitic strip to produce circular polarization and increased bandwidth for cylindrical dielectric resonator antenna," *Electron. Lett.*, vol. 37, pp. 406–408, Mar. 2001.
- [7] Z. Li, C. Wu, and J. Litva, "Adjustable frequency dielectric resonator antenna," *Electron. Lett.*, vol. 32, pp. 606–607, Mar. 1996.
- [8] Z. N. Chen, K. W. Leung, K. M. Luk, and E. K. N. Yung, "Effect of parasitic disk on a coaxial probe-fed dielectric resonator antenna," *Microw. Opt. Techn. Lett.*, vol. 15, no. 3, pp. 166–168, Jun. 1997.
- [9] H. K. Ng and K. W. Leung, "Excitation of CP aperture-coupled dielectric resonator antenna with a parasitic patch," in *IEEE Antennas and Propagation Soc. Int. Symp. Dig.*, vol. 4, Boston, MA, Jul. 2001, pp. 202–205.
- [10] K. W. Leung, W. C. Wong, and H. K. Ng, "Circularly polarized slot-coupled dielectric resonator antenna with a parasitic patch," *IEEE Antennas Wireless Propag. Lett.*, vol. 1, pp. 57–59, 2002.
- [11] K. W. Leung, K. M. Luk, K. Y. A. Lai, and D. Lin, "Theory and experiment of an aperture-coupled hemispherical dielectric resonator antenna," *IEEE Trans. Antennas Propag.*, vol. 43, pp. 1192–1198, Nov. 1995.
- [12] M. B. Oliver, Y. M. M. Antar, R. K. Mongia, and A. Ittipiboon, "Circularly polarized rectangular dielectric resonator antenna," *Electron. Lett.*, vol. 31, pp. 418–419, Mar. 1995.
- [13] K. P. Esselle, "Circularly polarized higher-order rectangular dielectric resonator antenna," *Electron. Lett.*, vol. 32, pp. 150–151, Feb. 1996.
- [14] C. Y. Huang, J. Y. Wu, and K. L. Wong, "Cross-slot-coupled microstrip antenna and dielectric resonator antenna for circular polarization," *IEEE Trans. Antennas Propag.*, vol. 47, no. 4, pp. 605–609, Apr. 1999.
- [15] K. W. Leung and S. K. Mok, "Circularly polarized dielectric resonator antenna excited by a perturbed annular slot with a backing cavity," *Electron. Lett.*, vol. 37, no. 15, pp. 934–936, Jul. 2001.
- [16] A. A. Kishk, B. Ahn, and D. Kajfez, "Broadband stacked dielectric resonator antennas," *Electron. Lett.*, vol. 25, pp. 1232–1233, Aug. 1989.
- [17] A. Sangiovanni, J. Y. Dauvignac, and C. Pichot, "Stacked dielectric resonator antenna for multifrequency operation," *Microw. Opt. Technol. Lett.*, vol. 18, pp. 303–306, Jul. 1998.
- [18] K. W. Leung, K. M. Luk, K. Y. Chow, and E. K. N. Yung, "Bandwidth enhancement of dielectric resonator antenna by loading a low-profile dielectric disk of very high permittivity," *Electron. Lett.*, vol. 33, pp. 725–726, Apr. 1997.
- [19] G. P. Junker, A. W. Glisson, and A. A. Kishk, "Input impedance of dielectric resonator antennas top loaded with high permittivity and conducting disks," *Microw. Opt. Technol. Lett.*, vol. 9, pp. 204–207, Jul. 1995.
- [20] R. N. Simons and R. Q. Lee, "Effect of parasitic dielectric resonators on CPW/aperture-coupled dielectric resonator antennas," in *Proc. Inst. Elect. Eng.*, vol. 140, Oct. 1993, pp. 336–338.
- [21] Z. Fan, Y. M. M. Antar, A. Ittipiboon, and A. Petosa, "Parasitic coplanar three-element dielectric resonator antenna subarray," *Electron. Lett.*, vol. 32, pp. 789–790, Apr. 1996.
- [22] K.-L. Wong, N.-C. Chen, and H.-T. Chen, "Analysis of a hemispherical dielectric resonator antenna with an airgap," *IEEE Microwave Guided Wave Lett.*, vol. 3, pp. 355–357, Oct. 1993.
- [23] K. W. Leung, "Complex resonance and radiation of hemispherical dielectric resonator antenna with a concentric conductor," *IEEE Trans. Microwave Theory Technol.*, vol. 49, no. 3, pp. 524–531, Mar. 2001.
- [24] N. C. Chen, H. C. Su, K. L. Wong, and K. W. Leung, "Analysis of a broad-band slot-coupled dielectric-coated hemispherical dielectric resonator antenna," *Microw. Opt. Technol. Lett.*, vol. 8, pp. 13–16, Jan. 1995.
- [25] S. M. Shum and K. M. Luk, "Numerical study of a cylindrical dielectric-resonator antenna coated with a dielectric layer," *Proc. Inst. Elect. Eng.-Microw. Antennas Propag.*, vol. 142, pp. 189–191, Apr. 1995.
- [26] A. A. Kishk, Y. Yin, and A. W. Glisson, "Conical dielectric resonator antennas for wide-band applications," *IEEE Trans. Antennas Propag.*, vol. 50, no. 4, pp. 469–474, Apr. 2002.
- [27] H. K. Ng and K. W. Leung, "Conformal-strip-excited dielectric resonator antenna with a parasitic strip," in *IEEE Antennas and Propagation Soc. Int. Symp. Dig.*, vol. 4, Salt Lake City, UT, Jul. 2000, pp. 2080–2083.



**Kwok Wa Leung** (S'90–M'93–SM'02) was born in Hong Kong on April 11, 1967. He received the B.Sc. degree in electronics and Ph.D. degree in electronic engineering from the Chinese University of Hong Kong, in 1990 and 1993, respectively.

From 1990 to 1993, he was a Graduate Assistant with the Department of Electronic Engineering, the Chinese University of Hong Kong. In 1994, he joined the Department of Electronic Engineering at City University of Hong Kong, Kowloon, as an Assistant Professor and became an Associate Professor in 1999. From 2001 to 2004, he was appointed the Programme Leader for BEng (Honors) in Electronic and Communication Engineering. His research interests include dielectric resonator antennas, microstrip antennas, wire antennas, numerical methods in electromagnetics, and mobile communications.

Dr. Leung received the URSI Young Scientists Awards in 1993 and 1995, awarded by XXIVth General Assembly of the International Union of Radio Science (URSI) and 15th URSI Triennial International Symposium on Electromagnetic Theory, respectively.



**Hoi Kuen Ng** was born in Hong Kong on April 10, 1975. He received the B.Sc. degree in information technology and the Ph.D. degree in electronic engineering from the City University of Hong Kong, Kowloon, in 1998 and 2003, respectively.

He is now a Senior Research Assistant at the City University of Hong Kong. His research interests include dielectric resonator antennas, circularly polarized antennas, and numerical methods in electromagnetics.